The PanK2 Genes of Mouse and Human Specify Proteins with Distinct Subcellular Locations

Roberta Leonardi[1], Yong-Mei Zhang[1], Athanasios Lydikis[2], Robert D. Stevens[3], Olga R. Ilkayeva[3], Brett R. Wenner[3], James R. Bain[3], Christopher B. Newgard[3], Charles O. Rock[1], and Suzanne Jackowski[1]

Department of Infectious Diseases, St Jude Children's Research Hospital, Memphis, Tennessee 38105[1], and Genome Biology Program DOE-Joint Genome Institute, Walnut Creek, California 94598[2], Sarah W. Stedman Nutrition and Metabolism Center, Duke University School of Medicine, Durham, North Carolina 27704[3]

¶Address correspondence to: Suzanne Jackowski, Ph.D., Department of Infectious Diseases, St Jude Children's Research Hospital, 332 N. Lauderdale, Memphis, Tennessee 38105-2794, Voice: 901 495-3494; Fax: 901 495-3099; Email: suzanne.jackowski@stjude.org

Abbreviations used are: CoA, coenzyme A; PanK, pantothenate kinase. Specific isoforms are numbered and preceded by 'm' for murine and 'h' for human; DTT, dithiothreitol; PBS, phosphate buffered saline; PKAN, PanK-associated neurodegeneration; PMSF, phenylmethylsulphonyl fluoride; qRT-PCR, real-time reverse transcriptase-polymerase chain reaction.

Running title: Regulation and localization of murine PanK2

Word count (Material and Methods) =

(Introduction, Results and Discussion) =

Keywords: pantothenate kinase, coenzyme A, mitochondria, neurodegeneration, acylcarnitine, and acetyl-CoA.

ABSTRACT

Coenzyme A (CoA) biosynthesis is initiated by pantothenate kinase (PanK) and tissue CoA levels are controlled through differential expression and allosteric regulation of the PanK isoforms. Mutations in human PanK2 (hPanK2) cause a neurodegenerative disorder termed PKAN; however, PKAN neuropathology is not recapitulated in *Pank2*$^{-/-}$ mice. The distribution of the PanK isoforms differed between human and mouse tissues with the relative expression of PanK2 being higher in human brain compared to mouse brain. Comparative genomics analysis revealed that the acquisition of a mitochondrial targeting signal was limited to the PanK2 sequences from primates, and mouse PanK2 was localized in the cytosol. Both human and mouse PanK2 possessed similar biochemical properties, responding to inhibition by acetyl-CoA and activation by palmitoylcarnitines. Mouse brain had an abundance of the PanK2 allosteric activators, long-chain acylcarnitines, compared to liver, suggesting that the PanK2 isoform is more catalytically active in brain compared to liver. CoA levels were the same in tissues from wild-type and *Pank2*$^{-/-}$ mice, and were highest in liver compared to brain and testes. The differences in the tissue-specific expression and cellular localization of the mouse PanK2 compared to human PanK2 may account for the inability to recapitulate the neuropathology of PKAN disease in the mouse model.

INTRODUCTION

CoA is an essential cofactor that plays a central metabolic role as the predominant acyl group carrier in living organisms (23). The intracellular CoA levels vary depending on the metabolic state of the cell and are tightly controlled to allow coordination of major anabolic and catabolic pathways such as the tricarboxylic acid cycle and fatty acid metabolism (23,35). Regulation of the cofactor concentration is achieved through feedback inhibition of pantothenate kinase (PanK), the first enzyme in the biosynthetic pathway (28,29,34). PanK catalyzes the ATP-dependent phosphorylation of pantothenate (vitamin B_5) to 4′-phosphopantothenate, and mammals express four catalytically active isoforms that have different sensitivities to inhibition by free CoA or CoA thioesters (30,40,41). A fifth potential isoform, PanK4, lacks the essential catalytic glutamate residue present in all other enzymes (9) and is not a functional pantothenate kinase (39). PanKs share a >80% identical catalytic core (10,30,40) attached to unrelated N-terminal extensions that range from a few residues in the case of PanK1β and PanK3 to ~100-200 residues in the case of PanK1α and PanK2. The N terminus of human PanK2 (hPanK2) directs it to the mitochondria. hPanK2 is sequentially processed twice to yield a stable 48 kDa mature protein (10,17,19). The sequences adjacent to the cleavage sites at residues 31 and 140, implicate the mitochondrial processing peptidase in both cleavage steps. A hPanK2 construct starting at Leu111 (42) lacks the first mitochondrial targeting signal, but is still processed and targeted to the mitochondria (17). Removal of both signals causes the enzyme to mislocalize to the cytosol (10,17). A catalytically active hPanK2 inside the mitochondria was irreconcilable with the high organelle CoA concentration (13,37) until the discovery of palmitoylcarnitine as a positive regulator of hPanK2 (22). Palmitoylcarnitine releases the acetyl-CoA inhibition by competing for its binding site, and this regulatory mechanism activates hPanK2 when the mitochondrial demand for CoA is high for β-oxidation.

Pantothenate kinase-associated neudrodegeneration (PKAN) is a rare autosomal recessive disease caused by mutations in the *PANK2* gene (7,42). PKAN patients exhibit pathological accumulation of iron in the brain, movement and speech defects and, in some cases, pigmentary

retinopathy (7,8,42). The classic form of the disease appears in childhood and is characterized by a relentless progression of dystonia, dysarthria and rigidity. The classical disease is more frequently associated with mutations that abolish or severely impair hPanK2 activity. The atypical form of PKAN has a later age at onset and a slower progression of speech-related and psychiatric symptoms. Some hPanK2 mutations result in protein misfolding or in truncated proteins; however, others give rise to proteins with wild-type or significant residual catalytic activity (19,41). Active hPanK2 mutants exhibit the same regulatory properties and localization as the wild-type enzyme (19,22,41), raising the question of what hPanK2 function is compromised by these mutations. To further complicate the picture, the connection between CoA biosynthesis/metabolism, neurodegeneration and brain iron accumulation remains unclear. Reduced phosphorylation of pantothenate may cause accumulation of cysteine, a CoA precursor, in regions of the brain that are normally rich in non-heme iron. Cysteine oxidation in the presence of iron would then result in free radical production and cell damage (17,42). Alternatively, oxidative stress caused by reduced CoA-dependent energy production may selectively impact those tissues like the retina and the brain characterized by a high metabolic demand and sensitivity to oxidative damage (7). There is a growing body of evidence supporting the role of mitochondria in the pathogenesis of several neurodegenerative diseases. Alzeihmer's, Parkinson's and Huntington's share common neurological features with PKAN (3,21,32,33) and mitochondrial defects lead to retinal degeneration (4,31,38) and male sterility (24,25).

A significant conundrum in the field is that the *Pank2* knockout mice do not recapitulate the neurological abnormalities that characterize the human phenotype, although they do exhibit retinal degeneration and male sterility (20). We addressed this issue by comparing the tissue distribution, gene structure, biochemical properties and subcellular localization of mPanK2 and hPanK2. Although the biochemical regulatory properties of the two enzymes are indistinguishable, differences in gene structure, subcellular localization of the proteins and relative abundance of PanK2 in human and murine tissues suggest rationales for the similarities and differences in the PKAN patients and *Pank2* knockout mice.

MATERIALS AND METHODS

Materials. Materials were purchased from the following suppliers: oligonucleotides and probes from the Hartwell Center at the St. Jude Children's Research Hospital; Poly(A)$^+$ RNAs from mouse and human brain sections, human liver, brain and testes from Clontech; molecular biology reagents from Qiagen; restriction enzymes and T4 DNA ligase from Promega; SuperScript™ II RNase H$^-$ reverse transcriptase, TRIZOL reagent, pCR2.1 and pcDNA3.1 vectors from Invitrogen; Real-time PCR mix from Applied Biosystems; Bradford dye-binding protein assay solution from Bio-Rad; D-[1-^{14}C]pantothenate (specific activity, 55 mCi/mmol) from American Radiolabeled Chemicals and [1-^{14}C]lauric acid (specific activity 55 mCi/mmol) from GE Healthcare. All other reagents were of analytical grade or better and were obtained from Sigma Chemical Co.

Generation of *Pank2* knockout mice. The targeting construct pPJ259 was generated by cloning 3 fragments of mouse *Pank2* genomic DNA into vector pNEOtkLoxP. pPJ259 contained a loxP site between a 3.5-kb genomic DNA and the TK and NEO selection cassettes, followed by a second loxP site upstream of a 2.8-kb genomic DNA fragment containing exon 3, and by a third one upstream of a 1.8-kb genomic DNA containing exon 4 (Fig. 1A). DraIII was used to linearize the targeting vector prior to transfection into the embryonic stem cell lines derived from 129/SVEV (Specialty Media), grown on mitotically inactivated mouse embryonic fibroblasts which carry resistance to neomycin. Clones resistant to G418 were selected and screened by Southern blot analysis using a 772-bp probe corresponding to a genomic DNA region outside the targeted portion. Genomic DNA (10 μg) from individual ES cell clones was digested with BamHI and Southern blot analysis was carried out as previously described (15). The presence of the third loxP site was confirmed by PCR analysis. ES cells containing the recombined *Pank2* DNA at the correct locus were injected into C57BL/6J blastocysts, which were then implanted into pseudopregnant female mice by the St. Jude Transgenic Core Facility. Male offspring with 75 to 90% agouti color, the coat color contributed by the ES cells, were bred with C57BL/6J females. Pups that were 100% agouti, indicating germ line transmission, were screened. Tail clips were lysed and multiplex PCR analysis was used to genotype the mice using RED Extract-N-Amp PCR

kit (Sigma) and three primers: F (TTCCCTGCTTAGGTAGGATTGC), R1 (CCTTTGGACACCATGTAAATGAAC) and T (CCAAGTTCGGGTGAAGGC). The wild type allele yielded a product of 618 bp, and the allele with the recombined *Pank2* yielded a product of 452 bp. FVB/N-Tg(ACTB-cre)2Mrt/J mice expressing Cre recombinase under the human β-actin gene promoter were utilized to generate complete deletion of *Pank2* by recombination of the first and third loxP sites, resulting in the deletion of exon 3. A multiplex PCR analysis was used to genotype the offsprings from the breeding of ACTB-cre mice with mice heterozygous for the recombined *Pank2* using primers F, R1 and R2 (CCTCAACTCCTAGATCCAAACTG). A 618 bp product indicated the presence of a wild type allele, and a 526 bp product indicated the presence of a knockout allele. Heterozygous mice for *Pank2* knockout were bred to generate homozygous knockout mice.

Real time qRT-PCR analysis. Total RNA was either purchased (mouse and human brain sections, human liver, brain and testes) or isolated from whole brain and caudate nucleus region, whole liver and testes of 2-3 wild type and *Pank2*$^{-/-}$ mice, using the TRIZOL reagent according to the manufacturer's instructions. Pelleted RNA was resuspended in nuclease-free water, digested with DNase I to remove any contaminating genomic DNA, aliquoted, re-precipitated in ethanol and stored at –20°C.

Synthesis of first-strand cDNA was obtained by reverse transcription using SuperScript™ II RNase H$^-$ reverse transcriptase, the RNA templates and random primers. Quantitative real-time PCR of the human and murine PanK isoforms in each sample was performed in triplicate using the ABI Prism® 7700 Sequence Detection System using primers and probes listed in Table 1. The Taqman Human GAPDH and Rodent GAPDH Control Reagents (Applied Biosystems) were the source of the primers and probes for quantitating the control GAPDH mRNA. All of the real-time values were compared using the C_T method, and the amount of cDNA ($2^{-\Delta CT}$) was reported relative to GAPDH.

Cloning of the murine *Pank2*, dell transfection and preparation of cell lysates. A 1.6 kb fragment encoding the long form of mPanK2 (10) was assembled from 3 ESTs (NCBI accession

154 numbers BG091057, CB247865 and BQ715345) and ligated into pcDNA3.1+ between EcoRI and
155 XbaI restriction sites. The resulting vector was named pPJ256.
156 HEK 293 and 293T cells were cultured in Dulbecco's modified Eagle's medium containing
157 10% fetal bovine serum (Atlanta Biologicals) and transfected with FuGENE 6 (Roche Applied
158 Science), as per manufacturer's instructions. For biochemical assays, 293T cells were transiently
159 transfected for 48 h with pPJ256 and pKM56, a pcDNA3.1-derived vector encoding the mature
160 hPanK2 (residues 141-570) (41). For immunofluorescence analysis, 293 cells were stably
161 transfected with pPJ256 and pKM4, a pcDNA3.1-derived vector encoding the mitochondrial
162 precursor hPanK2 (residues 1-570) (41), by selection in growth medium containing 600 μg/ml of
163 G418. Individual colonies were then expanded and screened for expression by western blotting
164 (see below). Transfected cells were collected, washed with PBS, and resuspended in lysis buffer
165 (10 mM Tris-HCl, pH 7.5, 1 mM EDTA, 10 mM NaF, and 5 μg/ml of leupeptin). After incubation on
166 ice for 1 h, cells were lysed by sonication. The lysate was centrifuged at 5,000 × *g* for 5 min at 4°C
167 to remove the unbroken cells. The supernatant was then either loaded on SDS-PAGE gels for
168 western blotting analysis or mixed with an equal volume of saturated ammonium sulfate for
169 subsequent activity assays. After incubation on ice for 1 h, the protein precipitate was collected by
170 centrifugation at 3,000 × *g* for 30 min. The precipitated protein was resuspended in the lysis buffer
171 without leupeptin and dialyzed against the same lysis buffer overnight at 4°C. The dialyzed protein
172 sample was stored in 50% glycerol at –20°C.
173 **Western blot detection and immunofluorescence.** Peptides corresponding to protein
174 stretches unique to mPanK2 (GESADSEARRRDPLRRR) and hPanK2 (EGRRQEPLRRRASSASV)
175 were synthesized and coupled to keyhole limpet hemocyanin by the Hartwell Center for
176 Biotechnology, St. Jude Children's Research Hospital, and sent to Rockland Inc. (Gilbertsville, PA)
177 to raise rabbit polyclonal antisera. Affinity purification of the polyclonal antibody was performed as
178 previously described (14,30). Heavy mitochondrial and cytosolic brain fractions (200 μg) were
179 loaded on 8% SDS-PAGE gels and the resolved proteins were electroblotted onto a polyvinylidene

difluoride membrane. The lysate from stably transfected cells (5 μg) was mixed with the same amount of cytosolic brain fraction from *Pank2* knockout mice and used as mPanK2 controls. mPanK2 was detected by the mPanK2 antibody at a concentration of 0.1 μg/ml. Horseradish peroxidase-conjugated protein A was used as the secondary antibody at a dilution of 1:5,000. The membranes were then stripped using a western blot recycling kit (Alpha Diagnostic International) and reprobed with antibodies against the mitochondrial marker pyruvate dehydrogenase (PDH, E2 subunit, Molecular Probes) and the cytosolic marker β-actin (Sigma) used at concentrations of 2.5 μg/ml and 5 μg/ml, respectively, using horseradish peroxidase-conjugated anti-mouse IgG (GE Healthcare) as secondary antibody at a dilution of 1:5,000. The immuno complexes were detected using the ECL kit (GE Healthcare).

The localization of mPanK2 and the mitochondrial precursor hPanK2 was determined by confocal microscopy, performed by the Scientific Imaging Shared Resource at St. Jude Children's Research Hospital using a Zeiss LSM 510 META multiphoton microscope equipped with a Plan-Neofluor 100x/1.3 oil immersion objective and controlled by Laser Scanning Microscope LSM 510 software (Ver.3.2, Carl Zeiss GmbH, Germany). Sample slides were prepared as described below and washed with PBS between each incubation step. HEK 293 cells stably transfected with pPJ256 and pKM4 were seeded in chamber slides (Lab-Tech II, Nalge Nunc International) and allowed to adhere and grow for 16-24 h before being incubated with 250 nM MitoTracker red CMXRos (Molecular Probes) for 30 min at 37°C. Cells were then fixed with 3.7% formaldehyde for 15 min at 37°C and permeabilized with 0.2% Triton X-100 for 5 min, before being incubated with the mPanK2 and hPanK2 antibodies at concentrations of 0.03 and 0.005 μg/ml, respectively, for 1 h at room temperature. Anti-rabbit IgG conjugated to Alexa Fluor 488 (Molecular Probes) diluted 1:250 was then added to the cells, followed by 1 h incubation at room temperature. The slides were finally washed with PBS and mounted with ProLong Gold antifade reagent with DAPI (Molecular Probes).

205 **Liver and brain fractionation.** Heavy mitochondria were isolated from wild type and
206 *Pank2* knockout mice liver or brain as described by Graham (6). All centrifugation steps and
207 fraction manipulation were conducted at 4°C. Briefly, freshly harvested organs from 4 wild type or
208 knock-out mice (~4 g) were homogenized in 12 ml of ice-cold LHM buffer (10 mM Hepes-KOH, pH
209 7.4, 0.2 M mannitol, 50 mM sucrose, 10 mM KCl and 1 mM EDTA) using a tissue grinder with a
210 motorized Teflon pestle (Glas-Col). The homogenate was centrifuged at 1,000 × *g* for 10 min to
211 remove nuclei, unbroken tissue and other cell debris. The supernatant was further centrifuged at
212 3,000 × *g* for 10 min and the pellet, consisting of heavy mitochondria, was washed twice with 10 ml
213 of LHM buffer, gently resuspended in 0.5 ml of the same buffer using a Dounce homogenizer and
214 finally aliquoted and stored at –80°C. The 3,000 × *g* supernatant was then sequentially centrifuged
215 at 12,000 × *g* for 15 min and 105,000 × *g* for 60 min to remove the light mitochondrial pellet and
216 microsomes, respectively. The resulting supernatant represented the cytosolic fraction.
217 **CoA measurements.** Extraction of CoA species from mouse whole tissues or liver
218 fractions and CoA assay were performed as described by Knights and Drew (18) with some
219 modifications. For whole liver, brain and testes, ~100 mg of tissue were homogenized in 0.4 ml of
220 chilled 6% $HClO_4$ containing 28 mM DTT. For liver fractions, 12 mg of mitochondrial or cytosolic
221 protein were mixed with an equal volume of 12% $HClO_4$ containing 56 mM DTT. The precipitated
222 proteins were removed by centrifugation and the pellet put aside for quantitation of long-chain CoA
223 thioesters. The supernatant was divided into two aliquots; one aliquot was adjusted to pH 7.5-8.5
224 with 2 M KOH and centrifuged to remove the insoluble potassium perchlorate formed, then used to
225 measure the amount of free CoA. The second aliquot was adjusted to pH 11-12 with 1 M KOH,
226 incubated for 1 h at room temperature to hydrolyze the short-chain CoA thioesters, then
227 neutralized with 0.6 M HCl and centrifuged. The supernatant was extracted 3 times with an equal
228 volume of hexane and the aqueous phase saved to determine the sum of free and short-chain
229 CoAs. The pellet containing the long-chain CoA thioesters from the first centrifugation step was
230 first washed with 0.6% perchloric acid containing 5 mM DTT, then with 5 mM DTT and finally

231 resuspended in the same solution. The CoA thioesters were hydrolyzed to free CoA and extracted
232 as described above. The reaction mixture for the CoA assay contained 200 mM Tris-HCl (pH 7.5),
233 8 mM $MgCl_2$, 0.1% Triton X-100, 2 mM EDTA, 20 mM NaF, 2.5 mM ATP, 10 μM [1-^{14}C]lauric acid,
234 100 ng of *E. coli* acyl-CoA synthetase (0.0863 U) and extracts containing 25-400 pmol of free CoA,
235 in a total volume of 100 μl. The reaction was initiated by the addition of the enzyme, and the
236 reaction mixture was incubated at 35°C for 30 min, followed by the addition of 325 μl of
237 methanol:chloroform:n-heptane (1.41/1.25/1, v/v/v) and 25 μl of 0.4 M acetic acid. After the
238 mixture was mixed vigorously and centrifuged, [1-^{14}C]lauryl-CoA in upper aqueous phase was
239 quantitated by counting in 3 ml of ScintiSafe 30% using Beckman LS 6500. The amount of free
240 CoA, short-chain and long chain acyl-CoA were combined and expressed as nmoles of total CoA/g
241 of wet tissue or nmoles of total CoA/g of protein in the case of liver mitochondrial and cytosolic
242 fractions.

243 **Acylcarnitine measurements.** Specimens of powdered liver and brain from wild type and
244 *Pank2*$^{-/-}$ mice were homogenized in deionized water, and tissue extracts were prepared as
245 previously described (2,16). Measurement of acylcarnitines was done by direct-injection
246 electrospray tandem mass spectrometry, using a Quattro Micro LC-MS system (Waters-
247 Micromass) equipped with a model HTS-PAL autosampler (Leap Technologies), a model 1100
248 HPLC solvent delivery system (Agilent Technologies) and a data system running MassLynx
249 software.

250 **Pantothenate kinase activity assay.** The lysates of transfected HEK 293T cells were
251 obtained and treated as described above prior to measuring the pantothenate kinase activity (41).
252 In particular, the reaction mixtures contained 45 μM D-[1-^{14}C]pantothenate (specific activity 27.5
253 mCi/mmol), 250 μM ATP pH 7.0, 10 mM $MgCl_2$, 0.1 M Tris-HCl pH 7.5 and 5 μg of protein. The
254 inhibitory effect of acetyl-CoA on the activity of mPanK2 and mature hPanK2 was determined by
255 including increasing concentrations of the compound in the reaction mixtures, as indicated. To
256 investigate the effect of palmitoylcarnitine on the acetyl-CoA inhibition, mPanK2- and hPanK2-

containing lysates were incubated with 62.5 and 93.8 nM of inhibitor, respectively, and increasing concentrations of palmitoylcarnitine, as indicated. The residual pantothenate kinase activity in *PanK2* knockout mice liver and brain cytosolic fractions was measured in reaction mixtures containing 45 μM D-[1-^{14}C]pantothenate, 2.5 mM ATP pH 7.0, 10 mM $MgCl_2$, 0.1 M Tris-HCl pH 7.5, increasing amounts of protein, as indicated, and incubated for 15 min at 37°C. The activity of the correspondent wild type fractions was determined in parallel under the same conditions.

Bioinfomatic analysis. Genomic sequences for human (chromosome 20, NT_011387.8), chimpanzee (chromosome 20, NW_001230484), cow (chromosome 13, NW_001493148.1), dog (chromosome 24 NW_876277.1), cat (no chromosome information, AANGO1231943.1) and mouse *PanK2* (chromosome 2, NW_000178.1) were retrieved from NCBI. The macaque genomic sequence was retrieved from the sequencing center's website (http://www.hgsc.bcm.tmc.edu/projects/rmacaque/). Sequence comparisons were performed using the VISTA tools for comparative genomics (http://genome.lbl.gov/vista/index.shtml) (5).

RESULTS

Generation of *Pank2* knockout mice. PanK2 knockout mice were first generated by insertion of a selection cassette and disruption of the *Pank2* coding sequence (20). We independently derived *Pank2*-deficient mice by deletion of a 2.8 kb DNA fragment containing exon 3 (Fig. 1A). Cre recombinase-dependent recombination of the first and third loxP sites resulted also in the removal of the selection cassette along with exon 3. Embryonic stem cells were transfected and selected, and chimeric mice were generated and bred by standard procedures described under "Materials and Methods." Mice heterozygous for *Pank2* were identified by PCR analysis of tail DNA and bred to produce homozygous knockout mice (Fig. 1B). A reproductive defect in the male PanK2-deficient mice precluded establishment of a homozygous breeding colony, and routine mating of heterozygotes and genotyping of the pups was necessary to propagate the *Pank2*$^{-/-}$ mice. The testis phenotype of the knockout mice generated by deletion of the *Pank2* gene was the same as described previously (20). Measurement of the testes weight and histological analysis revealed significantly smaller testes and the absence of elongated mature spermatozoa in the seminiferous tubules of these *Pank2* knockout mice (data not shown). Our *Pank2*$^{-/-}$ mice did not show a significant difference in weight at 6-8 weeks of age compared to littermate controls.

Tissue distribution of murine and human PanK isoforms. A considerable number of PKAN-causing *PANK2* mutations completely abolish hPanK2 enzymatic activity as a result of frameshifts and premature stops in the enzyme sequence (8,42). Similarly, deletion of the mouse *Pank2* exon 3 resulted in loss of enzymatic activity (see below). In spite of this, only retinal degeneration is common between some of the PKAN patients and *Pank2* knockout mice, while the neurodegeneration is unique to humans and the knockout mice exhibit azoospermia (20). We compared the mRNA expression levels of the murine and human PanK isoforms in brain, testes and in liver by quantitative RT-PCR. Expression of PanK4 was not taken into account because it does not exhibit PanK activity (39). *PANK1* transcripts (*PANK1*α + *PANK1*β) dominated human liver, whereas *Pank1* transcripts (*Pank1*α + *Pank1*β) in mouse liver were equivalent to *Pank3*

298 transcripts (Fig. 2) and relatively lower than in human. *PANK2* transcripts, on the other hand, were
299 relatively higher than *PANK1* and equivalent to *PANK3* in human brain, whereas *Pank2* transcripts
300 were low in mouse brain and *Pank3* expression was highest. *Pank2* transcripts were extremely
301 high in mouse testis, but were considerably less abundant in human testis. The ratio between
302 mouse *Pank2* and *Pank3* mRNAs was estimated at approximately 1:2 in brain and 1:1 in testes,
303 with *Pank2* representing 34% and 46% of the expressed isoforms in the two tissues, respectively
304 (Fig. 2A). Human *PANK2* transcripts were high in brain, equivalent to *PANK3,* and represented
305 45% of the *PANK* transcripts. Only 21% of the PanKs expressed in human testes were the *PANK2*
306 isoform (Fig. 2B). A detailed analysis of specific areas of the brain revealed a high expression of
307 human *PANK2* transcripts in the cerebellum, which controls motor coordination and movement,
308 and, as previously reported, in the caudate nucleus (10) (Fig. 2D). The overall abundance of the
309 murine *Pank* transcripts was lower than what was measured in the corresponding human brain
310 fractions (Fig. 2C), but the level of *Pank2* was higher in the cerebellum and cerebral cortex
311 compared to whole brain. These data revealed a correlation between the predominance of PanK2
312 expression and the physiological impact of loss of expression in tissues from human and mouse.

313 **PanK isoform expression and tissue CoA levels in wild-type and *Pank2* knockout**
314 **mice.** Loss of *Pank2* expression did not result in increased expression of either *Pank1* or *Pank3* in
315 the brain, testes or liver of *Pank2*$^{-/-}$ mice (data not shown). Measurements of the CoA content
316 revealed that brain and testes from adult wild type mice contained 19 and 26 nmoles of total CoA
317 per gram of wet tissue, respectively, while the liver content was 6-fold higher (Fig. 3A). In each
318 tissue, 80-90% of the CoA pool was unesterified or "free." No significant difference in the total or
319 free CoA content was found between organs from wild type and age-matched *Pank2* knockout
320 mice, indicating that the remaining PanK isoforms were able to maintain the CoA levels, even in
321 mouse testes. The CoA levels in mitochondria or cytosol also were the same in mouse wild-type
322 and knockout tissues, as exemplified by liver (Fig. 3B). These data indicated that loss of PanK2
323 expression did not reduce the CoA content, and that the activities of the PanK1 and PanK3
324 enzymes supplied the cellular CoA requirements of most cell types.

Biochemical properties of mPanK2 and tissue acylcarnitine measurements. The mature hPanK2 (residues 141-570, 47.4 kDa) is similar to the predicted size of mPanK2 (48.6 kDa). The N-terminus of the full length mPanK2 is 122 residues shorter than the full-length human homolog, therefore we compared the regulatory properties of mPanK2 and the mature hPanK2 expressed in the lysates of transfected HEK 293T cells. We found that the two enzymes were similarly inhibited by acetyl-CoA and de-inhibited by palmitoylcarnitine (Fig. 4). The acetyl-CoA IC_{50}s were estimated at 125 nM for hPanK2 and 62.5 nM for mPanK2, with slight variations from preparation to preparation, and the concentration of pamitoylcarnitine that maximally restored the activity was approximately 8 μM in both cases (Figs. 4A and 4B). Free carnitine and short-chain acylcarnitines are not activators of hPanK2 (22), and the latter species were the major components of the acylcarnitine pool in mouse liver obtained from animals fed standard chow (Fig. 6B). Conversely, the mouse brain contained significantly higher amounts of myristoyl, palmitoyl, stearyl and oleoylcarnitine (Fig. 5A). Organs from wild-type or *Pank2* knockout mice had comparable acylcarnitine distributions (Fig. 5). Taken together, these data indicated that hPanK2 and mPanK2 had the same biochemical properties in humans and mice and pointed out that the contribution of PanK2 to the total PanK activity in a specific tissue would depend on the molar ratio of inhibitors and activator(s).

Bioinformatic analysis of mammalian PanKs and localization of mPanK2 in stably transfected cells and brain fractions. The complete coding sequence and the intron-exon organization of the human *PANK2* gene was elucidated by Hörtnagel and coworkers (10) who found an ATG start codon upstream of the CTG codon originally proposed as the start of the hPanK2 coding sequence (42). The N-terminus of the full length hPanK2 protein contains a mitochondrial targeting sequence (residues 1-140), which is responsible for the subcellular localization of the enzyme and is encoded by exon 1. We compared the corresponding nucleotide sequences from six organisms (humans, macaques, cows, dogs, cats and mice) using the VISTA tools for comparative genomics (Fig. 6). The analysis revealed that while the macaque sequence encoded an intact mitochondrial targeting sequence, most of the aligned nucleotide regions from

mouse, cat, dog and cow were not translated due to the presence of in-frame stop codons or the absence of earlier start codons. In spite of the sequence similarity, the predicted ATG start codon in these organisms corresponded to residue 123 of hPanK2, thus excluding most of the mitochondrial targeting sequence. The targeting sequence was also found in the predicted chimpanzee PanK2 protein (NCBI accession number XP_001163366), which was not included in the VISTA analysis because of the poor quality of the DNA data in the region aligned. These data suggest that emergence of a mitochondrial targeting sequence occurred following the divergence of primates.

The bioinformatics data prompted us to re-examine the subcellular localization of hPanK2 and mPanK2. Stable cell clones overexpressing the full-length forms of hPanK2 and mPanK2 were generated, and the localization of the two proteins was investigated *in situ* by confocal immunofluorescence microscopy using mPanK2- and hPanK2-specific antibodies. Unlike the mitochondrial hPanK2 (Fig. 7, E-H), mPanK2 was found in the cytosol (Fig. 7, A-B). These results were the same in either the human cell line, HEK 293T (Fig. 7), or the mouse cell line, NIH 3T3 (data not shown). The subcellular location of mPanK2 was confirmed by western blotting analysis of cytosolic and mitochondrial fractions obtained from wild-type and knockout mouse brains and livers using the mPanK2-specific antibody, along with antibodies that recognize the β-actin marker protein for cytosol and the pyruvate dehydrogenase marker for mitochondria (Fig. 8A). mPanK2 was found exclusively in wild type cytosol, not in mitochondria, and the size of the endogenous protein matched the size of the full-length expressed mPanK2 predicted from genomic analysis (48.6 kDa).

To corroborate these results, we measured the total PanK activity in the cytosol and heavy mitochondrial fractions isolated from mouse brain and liver. PanK activity was detected in the cytosolic (Fig. 8A), but not in the mitochondrial fractions. The PanK enzymatic assay cannot discriminate between the various isoforms, but comparison of the cytosolic activity from wild-type and knockout mice showed a 10- and 2-fold reduction in knockout brain and liver, respectively, under the conditions described under Materials and Methods. The residual PanK activity in

knockout brain and liver was due to the expression of the PanK1 and PanK3 isoforms, and knockout brain showed a greater decrease in activity, consistent with the higher relative abundance of mPanK2 in wild-type brain (32%) compared to liver (9%) (Fig. 2A). The total PanK enzymatic activity in wild-type brain was almost as high as in liver, despite somewhat lower PanK expression levels (Fig. 2A), and showed a greater proportional decrease in the knockout brain, indicating a greater PanK2 contribution in this tissue, possibly due to a higher concentration of long-chain acylcarnitine activators (Fig. 5A).

DISCUSSION

A major finding of this study is that mouse PanK2 is a cytosolic protein in contrast to the mitochondrial localization of the human enzyme. The PanK2 proteins from human and mouse are homologous due to the strong similarity between their catalytic cores, and accordingly their biochemical and regulatory properties are similar. Both proteins are equivalently sensitive to feedback inhibition by acetyl-CoA, which is relieved by long-chain acylcarnitine (Fig. 4)(22). The amino terminal sequences of the PanK2s from human and mouse are distinctly different; however, and the mouse protein does not localize to the mitochondria (Figs. 7 and 8). In contrast to hPanK2, the analysis of the mPanK2 sequence with PSORTII (11) does not indicate a mitochondrial localization for the enzyme, but rather it is predicted to localize to the cytosol. The cytosolic location of mPanK2 was directly observed using in situ microscopy of stably expressed protein and was confirmed by subcellular fractionation of the endogenous PanK2 in mouse brain and liver (Figs.7 and 8). mPanK2 is not processed and the molecular size of mPanK2 in vivo corresponds to the size predicted by expression from the first in-frame Met codon (48.6 kDa), rather than an upstream Leu codon (50.2 kDa) that was initially proposed as the start site (17). These data are not in agreement with previous reports that concluded both mouse and human PanK2 proteins as associated with mitochondria based on the immunolocalization of hPanK2 and mPanK2 in transiently transfected COS7 cells and tissue sections. However, our examination of the same data suggest a significant difference between the localization of the two proteins (17,20).

406 Analysis of the PanK2 protein sequences from available mammalian genomes shows that only
407 primates evolved the mitochondrial targeting mechanism, suggesting that this feature is related to
408 the more complex neurological development in primates.

409 These results provide a rationale for why the phenotype of the *Pank2* knockout mouse does
410 not include an overt neurological disease that is characteristic of PKAN patients, including those
411 with null mutations in the *PANK2* gene (20). The possibility of interference of the gene insertion
412 cassette on the transcriptional activity of flanking chromosomal regions was ruled out by the
413 independent isolation of a *Pank2*$^{-/-}$ mouse using a gene deletion strategy that removed the
414 selection cassette as well as exon 3. The loss of mPanK2 activity in *Pank2*$^{-/-}$ mice is not
415 accompanied by an increase in the expression level of the other isoforms, and does not lead to
416 decreased CoA levels in brain, liver or testes. These data indicate that the other PanK isoforms
417 are able to maintain the homeostatic cofactor concentration in most tissues of the knockout
418 animals. This outcome is not completely unexpected since all PanKs are regulated through
419 feedback inhibition by CoA thioesters and a drop in the inhibitor levels would stimulate the activity
420 of the remaining isoforms. However, the fact that the *Pank2* knockout mice exhibit a defect in
421 sperm maturation suggests cell-type specific isoform expression has a selective effect on
422 development of selected lineages. No data are available on the CoA content in normal and PKAN-
423 affected brains, although like the mouse testis, these data may not reveal deficiencies in
424 specialized cell types. There was a correlation between the relative abundance of PanK2
425 transcripts and the tissue-specific dysfunction related to the loss of its expression. Mouse PanK2
426 constituted a smaller proportion of the mRNA species in most brain regions compared to the
427 predominant expression of hPanK2 in human brain. In particular, the human caudate nucleus,
428 which is part of the basal ganglia where iron accumulation is noted in many PKAN patients (36),
429 has a high proportion of *PANK2* transcripts, whereas the mouse caudate nucleus has a relatively
430 lower amount (Fig. 2C). On the other hand, *Pank2* expression is high in mouse testes (Fig. 2A),
431 where loss of its expression impacted the development of spermatozoa in the knockout animals.

The intramitochondrial concentration of CoA species is estimated to be in the millimolar range, thousands of fold higher than what would inhibit the PanK2 enzymes (13,37). Carnitine is also an abundant metabolite (12) and this pool is made up of free carnitine, short- and long-chain carnitine esters. Compositional analysis of the acylcarnitines present in mouse liver and brain revealed a higher long-chain to short-chain ratio in the brain, suggesting that in non-stressed conditions on a standard diet, the basal activity of mPanK2 is higher in brain due to the higher concentration of activator. The ratio of free carnitine to acylcarnitine varies also as a function of the availability of fatty acids destined for β-oxidation and energy production (26,27). The cytosolic location of mPanK2 would not prevent its activation by acylcarnitine, but also would not optimize the response. In the absence of PanK2 expression, a prompt response to the mitochondrial demand for CoA may not be satisfied, potentially disrupting or delaying the function of the organelle, particularly in human neural tissue where the PanK2 is highly expressed and localizes to the site of palmitoylcarnitine synthesis. We recently proposed a model that places hPanK2 in the intramembrane space (22), the submitochondrial compartment where palmitoyl-CoA is converted to palmitoylcarnitine; the high local concentration of palmitoylcarnitine would efficiently activate hPanK2 making the enzyme a more sensitive sensor of the mitochondrial demand for CoA. However, because palmitoylcarnitine diffuses into the cytosol, the same sensory mechanism would work even if the enzyme is localized in this compartment, as is the case with mPanK2 and all other metazoan PanKs, with the exception of primates. Therefore, our working hypothesis is that the biochemical function of mPanK2 and hPanK2 is the same and does not strictly require mitochondrial localization.

Chemical knockout of the total PanK activity dramatically reduces CoA levels in liver and significantly affects mitochondrial function and morphology (39). Reduction or elimination of PanK2 activity in PKAN patients results in neurological symptoms that are common to several other neurodegenerative disorders associated with mitochondrial dysfunction (21,32,33). This correlation between potential mitochondrial dysfunction and hPanK2 activity has been attributed to the unique localization of hPanK2 (10,19). However, defects in mitochondrial respiration or

alteration of the transmembrane potential can also be the underlying cause of the male sterility and retinal degeneration (4,24,25,31,38) observed in the *Pank2* knockout mice (20) and the *fumble* fly (1), both of which are deficient in a cytosolic enzyme. Thus, it appears that this correlation is not linked to the specific localization of PanK2. Instead, knocking out of a PanK isoform would likely cause a mitochondrial dysfunction-related phenotype in cell types where the expression of one isoform predominates and the corresponding reduction in CoA level is less likely to be restored by the activation of the remaining isoforms.

ACKOWLEDGEMENTS

We thank Pamela Jackson, Karen Miller, Caroline Pate, Jina Wang and Ruobing Zhou, for their expert technical assistance. This work was supported by National Institutes of Health Grants GM 62896 (S.J.), DK58398 (C.B.N.), Cancer Center (CORE) Support Grant CA 21765, and the American Lebanese Syrian Associated Charities.

REFERENCES

1. **Afshar, K., P. Gonczy, S. DiNardo, and S. A. Wasserman**. 2001. *fumble* encodes a pantothenate kinase homolog required for proper mitosis and meiosis in Drosophila melanogaster. Genetics **157:**1267-1276.
2. **An, J., D. M. Muoio, M. Shiota, Y. Fujimoto, G. W. Cline, G. I. Shulman, T. R. Koves, R. Stevens, D. Millington, and C. B. Newgard**. 2004. Hepatic expression of malonyl-CoA decarboxylase reverses muscle, liver and whole-animal insulin resistance. Nat. Med. **10:**268-274.
3. **Dobson, J.** 2004. Magnetic iron compounds in neurological disorders. Ann. N. Y. Acad. Sci. **1012:**183-192.
4. **Finsterer, J.** 2006. Central nervous system manifestations of mitochondrial disorders. Acta Neurol. Scand. **114:**217-238.
5. **Frazer, K. A., L. Pachter, A. Poliakov, E. M. Rubin, and I. Dubchak**. 2004. VISTA: computational tools for comparative genomics. Nucleic Acids Res. **32:**W273-W279.
6. **Graham, J. M.** 1999. Isolation of Mitochondria from Tissues and Cells by Differential Centrifugation, p. 3.3.1-3.3.15. *In* J. S. Bonifacino, M. Dasso, J. B. Harford, J. Lippincott-Schwartz, and K. M. Yamada (ed.), Current Protocols in Cell Biology. John Wiley & Sons, Inc..
7. **Hayflick, S. J.** 2003. Unraveling the Hallervorden-Spatz syndrome: pantothenate kinase-associated neurodegeneration is the name. Curr. Opin. Pediatr. **15:**572-577.
8. **Hayflick, S. J., S. K. Westaway, B. Levinson, B. Zhou, M. A. Johnson, K. H. Ching, and J. Gitschier**. 2003. Genetic, clinical, and radiographic delineation of Hallervorden-Spatz syndrome. N. Engl. J. Med. **348:**33-40.
9. **Hong, B. S., M. K. Yun, Y.-M. Zhang, S. Chohnan, C. O. Rock, S. W. White, S. Jackowski, H. W. Park, and R. Leonardi**. 2006. Prokaryotic type II and type III pantothenate kinases: The same monomer fold creates dimers with distinct catalytic properties. Structure **14:**1251-1261.
10. **Hörtnagel, K., H. Prokisch, and T. Meitinger**. 2003. An isoform of hPANK2, deficient in pantothenate kinase-associated neurodegeneration, localizes to mitochondria. Hum. Mol. Genet. **12:**321-327.
11. **Horton, P. and K. Nakai**. 1997. Better prediction of protein cellular localization sites with the k nearest neighbors classifier. Proc. Int. Conf. Intell. Syst. Mol. Biol. **5:**147-152.
12. **Hutter, J. F., C. Alves, and S. Soboll**. 1990. Effects of hypoxia and fatty acids on the distribution of metabolites in rat heart. Biochim. Biophys. Acta **1016:**244-252.
13. **Idell-Wenger, J., L. Grotyohann, and J. R. Neely**. 1978. Coenzyme A and carnitine distribution in normal and ischemic hearts. J. Biol. Chem. **253:**4310-4318.
14. **Jackowski, S.** 1994. Coordination of membrane phospholipid synthesis with the cell cycle. J. Biol. Chem. **269:**3858-3867.
15. **Jackowski, S., J. E. Rehg, Y.-M. Zhang, J. Wang, K. Miller, P. Jackson, and M. A. Karim**. 2004. Disruption of CCTβ2 expression leads to gonadal dysfunction. Mol. Cell. Biol. **24:**4720-4733.
16. **Jensen, M. V., J. W. Joseph, O. Ilkayeva, S. Burgess, D. Lu, S. M. Ronnebaum, M. Odegaard, T. C. Becker, A. D. Sherry, and C. B. Newgard**. 2006. Compensatory responses to pyruvate carboxylase suppression in islet β-cells: preservation of glucose-stimulated insulin secretion. J. Biol. Chem. **281:**22341-22351.
17. **Johnson, M. A., Y. M. Kuo, S. K. Westaway, S. M. Parker, K. H. Ching, J. Gitschier, and S. J. Hayflick**. 2004. Mitochondrial localization of human PANK2 and hypotheses of secondary iron accumulation in pantothenate kinase-associated neurodegeneration. Ann. N. Y. Acad. Sci. **1012:**282-298.
18. **Knights, K. M. and R. Drew**. 1988. A radioisotopic assay of picomolar concentrations of coenzyme A in liver tissue. Anal. Biochem. **168:**94-99.
19. **Kotzbauer, P. T., A. C. Truax, J. Q. Trojanowski, and V. M. Y. Lee**. 2005. Altered neuronal mitochondrial coenzyme A synthesis in neurodegeneration with brain iron accumulation caused by abnormal processing, stability, and catalytic activity of mutant pantothenate kinase 2. J. Neurosci. **25:**689-698.
20. **Kuo, Y. M., J. L. Duncan, S. K. Westaway, H. Yang, G. Nune, E. Y. Xu, S. J. Hayflick, and J. Gitschier**. 2005. Deficiency of pantothenate kinase 2 (*Pank2*) in mice leads to retinal degeneration and azoospermia. Hum. Mol. Genet. **14:**49-57.
21. **Kwong, J. Q., M. F. Beal, and G. Manfredi**. 2006. The role of mitochondria in inherited neurodegenerative diseases. J. Neurochem. **97:**1659-1675.
22. **Leonardi, R., C. O. Rock, S. Jackowski, and Y.-M. Zhang**. 2007. Activation of human mitochondrial pantothenate kinase 2 by palmitoylcarnitine. Proc. Natl. Acad. Sci. U. S. A. **104:**1494-1499.

23. **Leonardi, R., Y.-M. Zhang, C. O. Rock, and S. Jackowski**. 2005. Coenzyme A: Back in action. Prog. Lipid Res. **44:**125-153.
24. **Nakada, K., A. Sato, K. Yoshida, T. Morita, H. Tanaka, S. Inoue, H. Yonekawa, and J. Hayashi**. 2006. Mitochondria-related male infertility. Proc. Natl. Acad. Sci. U. S. A. **103:**15148-15153.
25. **Perl, A., Y. Qian, K. R. Chohan, C. R. Shirley, W. Amidon, S. Banerjee, F. A. Middleton, K. L. Conkrite, M. Barcza, N. Gonchoroff, S. S. Suarez, and K. Banki**. 2006. Transaldolase is essential for maintenance of the mitochondrial transmembrane potential and fertility of spermatozoa. Proc. Natl. Acad. Sci. U. S. A. **103:**14813-14818.
26. **Ramsay, R. R. and A. Arduini**. 1993. The carnitine acyltransferases and their role in modulating acyl-CoA pools. Arch. Biochem. Biophys. **302:**307-314.
27. **Ramsay, R. R. and V. A. Zammit**. 2004. Carnitine acyltransferases and their influence on CoA pools in health and disease. Mol. Aspects Med. **25:**475-493.
28. **Robishaw, J. D., D. A. Berkich, and J. R. Neely**. 1982. Rate-limiting step and control of coenzyme A synthesis in cardiac muscle. J. Biol. Chem. **257:**10967-10972.
29. **Robishaw, J. D. and J. R. Neely**. 1984. Pantothenate kinase and control of CoA synthesis in heart. Am. J. Physiol. Cell. **246:**H532-H541.
30. **Rock, C. O., M. A. Karim, Y.-M. Zhang, and S. Jackowski**. 2002. The murine *Pank1* gene encodes two differentially regulated pantothenate kinase isozymes. Gene **291:**35-43.
31. **Sano, Y., A. Furuta, R. Setsuie, H. Kikuchi, Y. L. Wang, M. Sakurai, J. Kwon, M. Noda, and K. Wada**. 2006. Photoreceptor cell apoptosis in the retinal degeneration of Uchl3-deficient mice. Am. J. Pathol. **169:**132-141.
32. **Schapira, A. H.** 2002. Primary and secondary defects of the mitochondrial respiratory chain. J. Inherit. Metab. Dis. **25:**207-214.
33. **Schapira, A. H.** 2006. Mitochondrial disease. Lancet **368:**70-82.
34. **Song, W.-J. and S. Jackowski**. 1994. Kinetics and regulation of pantothenate kinase from *Escherichia coli*. J. Biol. Chem. **269:**27051-27058.
35. **Tahiliani, A. G. and C. J. Beinlich**. 1991. Pantothenic acid in health and disease. Vitam. Horm. **46:**165-228.
36. **Thomas, M., S. J. Hayflick, and J. Jankovic**. 2004. Clinical heterogeneity of neurodegeneration with brain iron accumulation (Hallervorden-Spatz syndrome) and pantothenate kinase-associated neurodegeneration. Mov. Disord. **19:**36-42.
37. **Williamson, J. and B. Corkey**. 1979. Assay of citric acid cycle intermediates and related compounds-uptake with tissue metabolite levels and intracellular distribution. Methods Enzymol. **55:**200-222.
38. **Zhang, X., D. Jones, and F. Gonzalez-Lima**. 2002. Mouse model of optic neuropathy caused by mitochondrial complex I dysfunction. Neurosci. Lett. **326:**97-100.
39. **Zhang, Y.-M., S. Chohnan, K. G. Virga, R. D. Stevens, O. R. Ilkayeva, B. R. Wenner, J. R. Bain, C. B. Newgard, R. E. Lee, C. O. Rock, and S. Jackowski**. 2007. Chemical knockout of pantothenate kinase reveals the metabolic and genetic program responsible for hepatic coenzyme A homeostasis. Chem. Biol. **14:**291-302.
40. **Zhang, Y.-M., C. O. Rock, and S. Jackowski**. 2005. Feedback regulation of murine pantothenate kinase 3 by coenzyme A and coenzyme A thioesters. J. Biol. Chem. **280:**32594-32601.
41. **Zhang, Y.-M., C. O. Rock, and S. Jackowski**. 2006. Biochemical properties of human pantothenate kinase 2 isoforms and mutations linked to pantothenate kinase-associated neurodegeneration. J. Biol. Chem. **281:**107-114.
42. **Zhou, B., S. K. Westaway, B. Levinson, M. A. Johnson, J. Gitschier, and S. J. Hayflick**. 2001. A novel pantothenate kinase gene (*PANK2*) is defective in Hallervorden-Spatz syndrome. Nat. Genet. **28:**345-349.

579

580 **TABLE I**

581 **Primers and Probes for mouse and human PanK RT-PCR**

582

Gene	Forward Primer (5′-3′)	Reverse Primer (5′-3′)	Probe (5′-3′)[1]
Pank1	ATGACTTGCCCTCATTTGCAT	TGGGAGCCCCTCCAAATT	CCGTATGAAGGGCAGCAAACCC
Pank2	TTGGGCATACGTGGAGCTTT	TCTCACATACATTTCAACAGGACAAG	TGGACTCCCACCAGCAGCTGAC
Pank3	CTAAGGAACGCCTGCCATTC	CTTTGGTTCCCAGTGACAGACA	AGCTGATCCAGAAACCGCAGTCA
PANK1	TGAGCTTATTGTTGAAAGGGATTTT	GGTGCTCAGAAGGCAGAGAAA	AGGACAGAACAATTACTCCATGAT GAATCTTC
PANK2	AGAGCTGCTCTGTGTTCAGTTGA	CGCATAGTAGCCTGCCTTACATT	AGCAAGTTCAAACAGGACACAAAA CCA
PANK3	CACCATGCTCTTATCTCGCACTT	TTGAAGGCAGAGGGCTCAAC	TCCCCTTGCCTGAATCTGG

583 [1]All probes used 6-FAM (6-carboxyfluorescein) as reporter and BHQ1 (black hole quencher 1) as

584 quencher.

FIGURE LEGENDS

FIG. 1. Generation of *Pank2* knockout mice by homologous recombination and cre-mediated deletion. (A) Organization of the *Pank2* locus and screening strategy for the targeting construct. ES cells containing the recombinant *Pank2* at the correct locus were identified by Southern blotting analysis using the BamHI restriction enzyme, B, and a 722 bp probe outside the targeted portion. LoxP sites (▶) allowed for the cre-mediated deletion of the selection cassette and exon 3. (B) Genotyping was accomplished by PCR using primers F, R and R2 as described under "Materials and Methods." A 618 and 526 bp products indicated the presence of a wild type allele and knockout allele, respectively.

FIG. 2. PanK isozyme expression in murine and human tissues. (A and B) The abundance of murine (A) or human (B) PanK isoform mRNAs was determined in brain, testes and liver by real time RT-PCR. (C and D) The same analysis was conducted on mRNA from specific regions of the murine (C) and human (D) brain. PanK2 is highly abundant in mouse testes and human brain. All RNA samples were purchased with the exception of murine RNA from whole brain, testes and liver and caudate nucleus that was extracted from 2-3 wild type mice as described under "Materials and Methods." Individual samples were analyzed in triplicate, averaged and plotted relative to mouse or human glyceraldehyde-3-phosphate dehydrogenase mRNA. Data obtained from different mice were then further averaged. All data are plotted as mean ± the standard error.

FIG. 3. Measurement of total CoA in murine whole tissues and liver fractions. (A) Total CoA levels were determined in brain, liver and testes obtained from wild type (black bars) and *Pank2* knockout (white bars) mice as described under Materials and Methods." (B) Mitochondrial and cytosolic fractions were isolated from the livers of wild type (black bars) and *Pank2* knockout (white bars) mice and the total CoA measured. No significant difference was observed CoA levels

610 of whole tissues or liver fractions from wild type and *Pank2*-deficient mice. The data represent the
611 average of three independent experiments ± the standard error.
612
613 **FIG. 4.** Regulatory properties of mPanK2 and hPank2. (A) Acetyl-CoA inhibited both
614 mPanK2 (●) and the mature form of hPanK2 (41) (○) with similar IC_{50} of 62.5 and 125 nM,
615 respectively. (B) Inhibition by acetyl-CoA was released by the addition of palmitoylcarnitine. The
616 enzymes were incubated with fixed concentrations of acetyl-CoA corresponding to the respective
617 IC_{50}s and with increasing amounts of the activator. The data represent the average of two
618 independent experiments ± the standard error.
619
620 **FIG. 5.** Analysis of the acylcarnitine pool in mouse tissues. The composition of the
621 acylcarnitine pool present in the brain (A) and liver (B) of wild type and *Pank2* knockout mice was
622 determined by electrospray mass spectroscopy as described under "Materials and Methods." The
623 brain and liver acylcarnitine pools showed significantly different compositions, with long-chain
624 acylcarnitines, known activators of PanK2, were abundant in the brain but not in the liver. Loss of
625 mPanK2 did not cause a remodeling of the acylcarnitine pool.
626
627 **FIG. 6.** DNA level sequence similarity of the 5-untranslated regions and exon 1 of six
628 mammals. Genomic DNA sequences were aligned using the VISTA set of tools for comparative
629 genomics and using human *PANK2* as the reference sequence. Black arrows indicate the
630 positions of the predicted start codons in the corresponding organisms. The region corresponding
631 to the human mitochondrial targeting signal has been shadowed and the positions of the
632 mitochondrial processing peptidase cleavage sites (19) are indicated by the scissor symbol at the
633 top.
634
635 **FIG. 7.** Subcellular localization of mPanK2 and hPanK2. (A-C) Stably transfected HET 293
636 cells expressing mPanK2, (E-G) the mitochondrial precursor form of hPanK2 (41) or containing (D

637 and H) the empty vector were cultured and prepared for immunofluorescence as described under
638 'Materials and Methods'. (A and D) Cells were incubated with MitoTracker red CMXRos and with
639 specific antibodies against (B and F) mPanK2 or (E and H) hPanK2, followed by incubation with
640 anti-rabbit IgG conjugated to Alexa Fluor 488 green; nuclei were stained with DAPI (blue). Panels
641 C and D show the merged images for mPanK2 and empty vector, respectively; panels G and H
642 show the merged images for hPanK2 and empty vector, respectively. hPanK2 localized to the
643 mitochondria, while mPanK2 was found in the cytosol.
644
645 **FIG. 8.** Cytosolic localization of mPanK2 confirmed by activity assays and western blotting
646 analysis. (A) Western blot using 200 μg of brain mitochondrial and cytosolic fraction protein from
647 wild type and *Pank2* knockout mice and the specific mPanK2 antibody. 195 μg of cytosolic protein
648 from knockout mice were mixed with 5 μg of lysate protein from stably transfected HET 293 cells
649 expressing mPanK2 and used as a control. (B) The total PanK activity was measured in liver (■,
650 □) and brain (●, ○) cytosolic fractions obtained from wild type (■, ●) and *PanK2* knockout (□, ○)
651 mice as described under 'Materials and Methods'. Cytosolic fractions from knockout mice showed
652 a significantly lower activity than those from wild type, consistent with the absence of mPanK2 in
653 this cellular compartment.

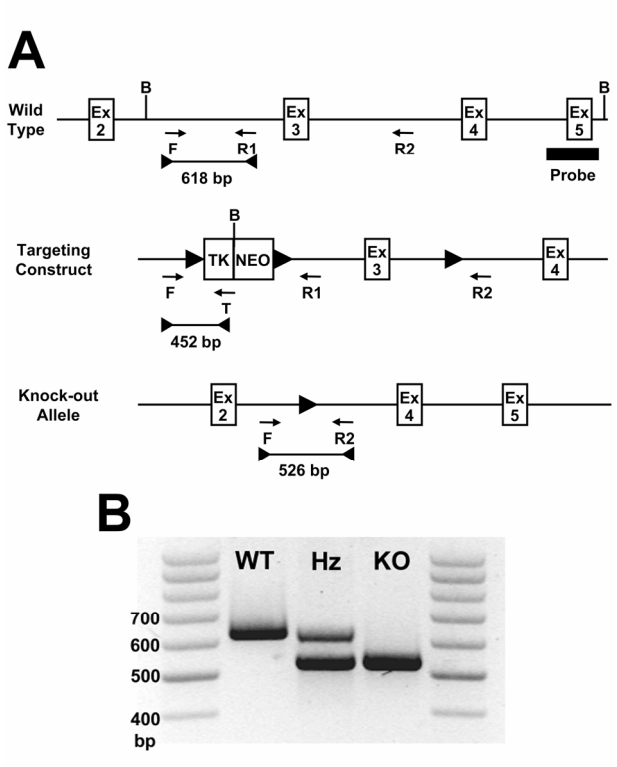
A
Wild Type
B
Ex 2
Ex 3
Ex 4
Ex 5
B
F
R1
R2
618 bp
Probe
Targeting Construct
B
TK
NEO
Ex 3
Ex 4
F
T
R1
R2
452 bp
Knock-out Allele
Ex 2
Ex 4
Ex 5
F
R2
526 bp
B
WT
Hz
KO
700
600
500
400
bp

Figure 1

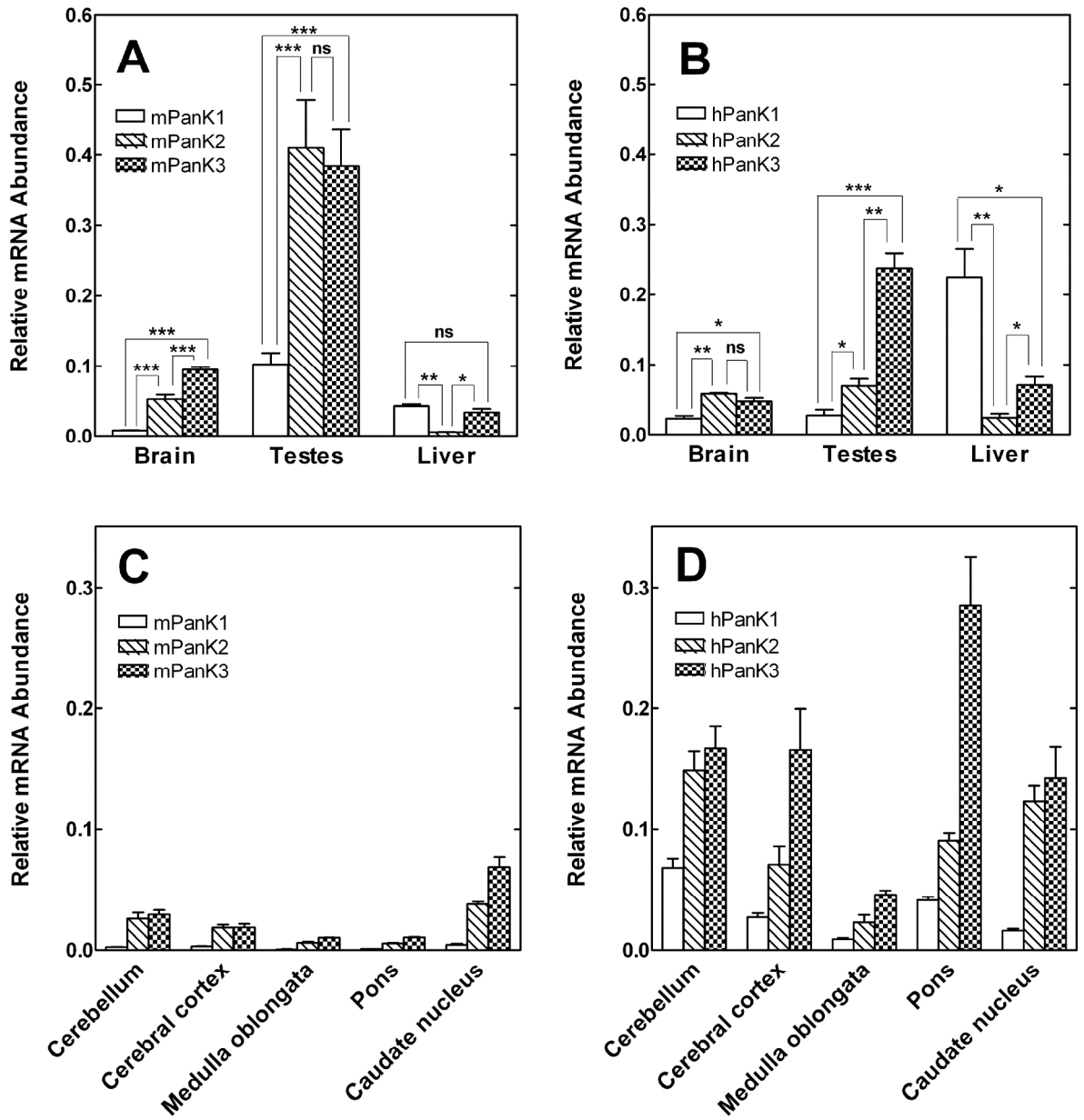
A
mPanK1
mPanK2
mPanK3
Relative mRNA Abundance
Brain
Testes
Liver
ns
B
hPanK1
hPanK2
hPanK3
C
D
Cerebellum
Cerebral cortex
Medulla oblongata
Pons
Caudate nucleus

Figure 2

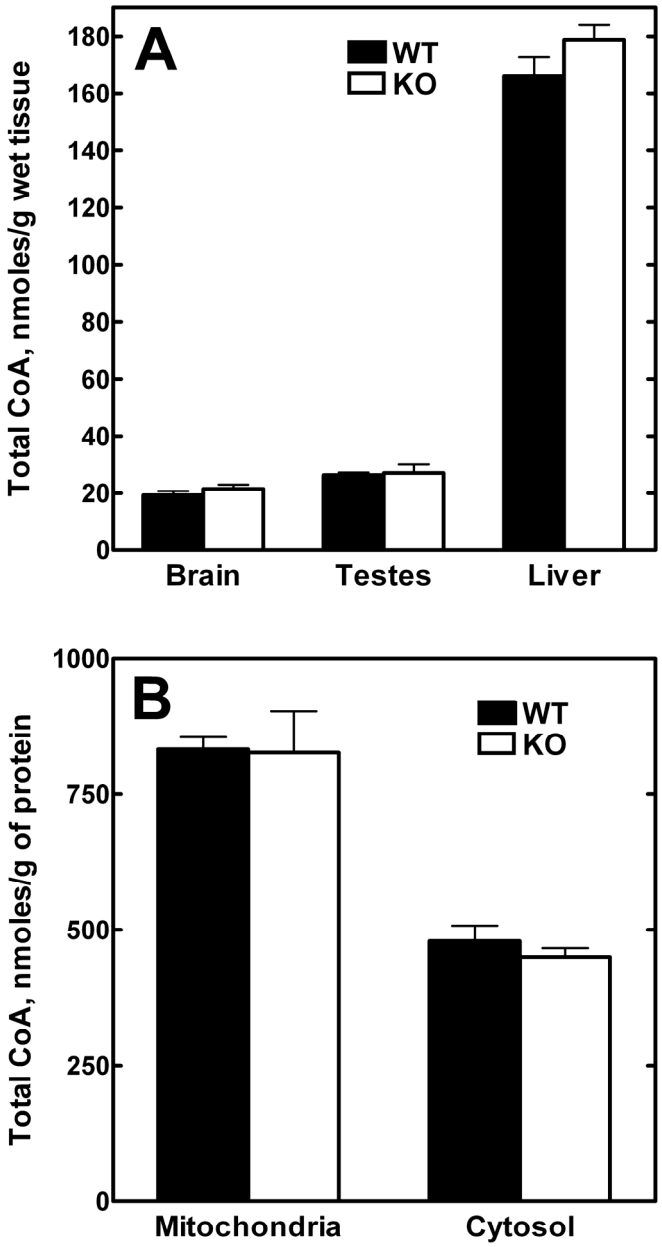

673

674 **Figure 3**

675

676

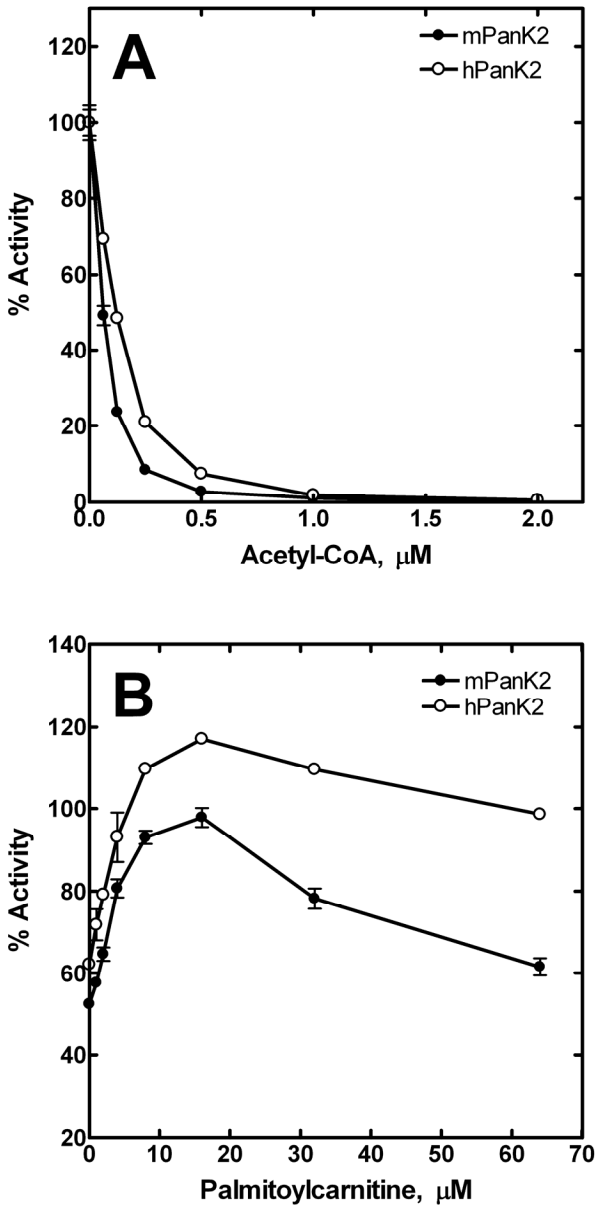

677

678 **Figure 4**

679

680

681

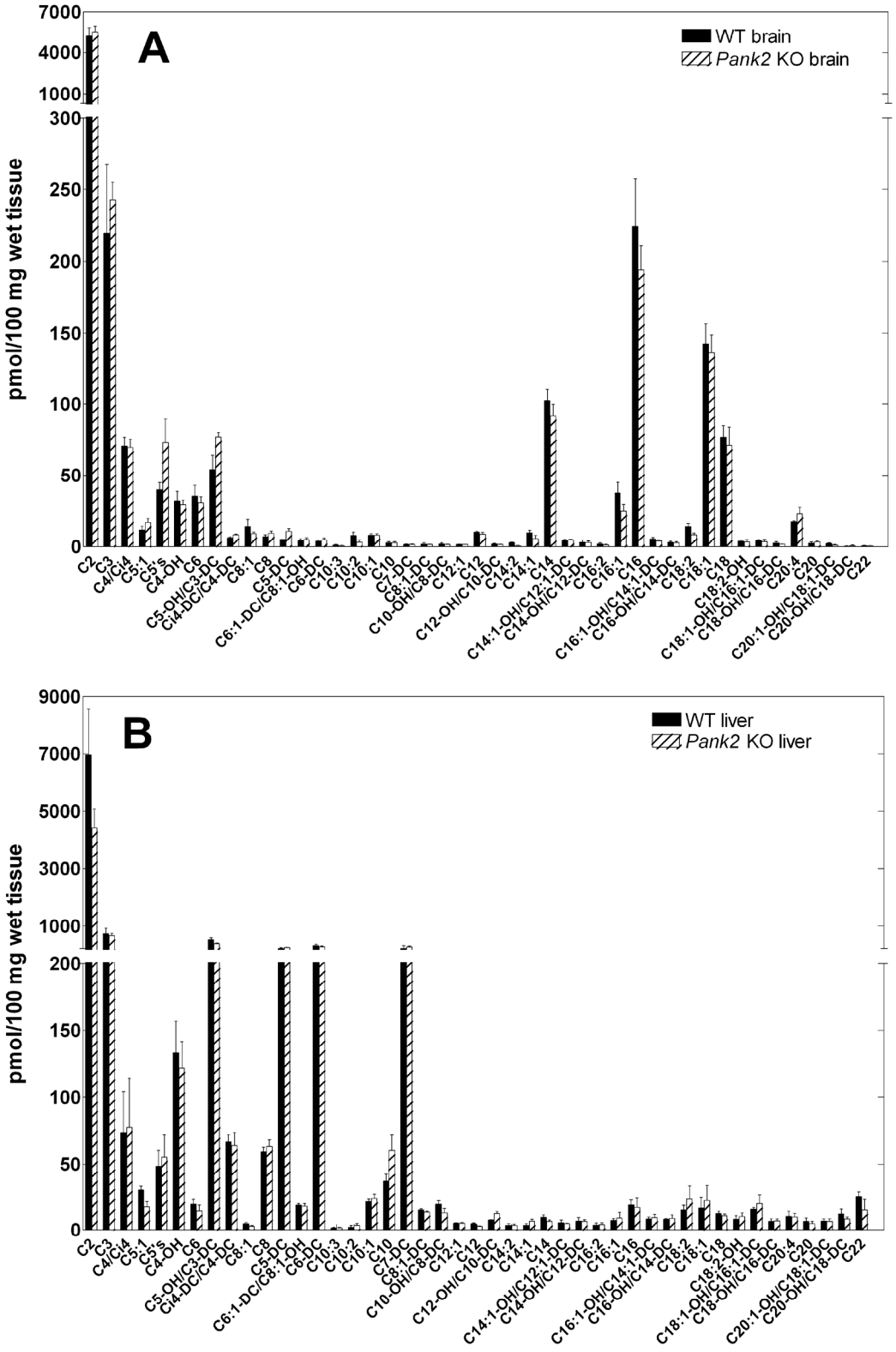
A
WT brain
Pank2 KO brain
pmol/100 mg wet tissue
7000
4000
1000
300
250
200
150
100
50
0
C2
C3
C4/Ci4
C5:1
C5's
C4-OH
C6
C5-OH/C3-DC
Ci4-DC/C4-DC
C8:1
C8
C5-DC
C6:1-DC/C8:1-OH
C6-DC
C10:3
C10:2
C10:1
C10
C7-DC
C8:1-DC
C10-OH/C8-DC
C12:1
C12
C12-OH/C10-DC
C14:2
C14:1
C14
C14:1-OH/C12:1-DC
C14-OH/C12-DC
C16:2
C16:1
C16
C16:1-OH/C14:1-DC
C16-OH/C14-DC
C18:2
C18:1
C18
C18:2-OH
C18:1-OH/C16:1-DC
C18-OH/C16-DC
C20:4
C20
C20:1-OH/C18:1-DC
C20-OH/C18-DC
C22
B
WT liver
Pank2 KO liver
pmol/100 mg wet tissue
9000
7000
5000
3000
1000
200
150
100
50
0
C2
C3
C4/Ci4
C5:1
C5's
C4-OH
C6
C5-OH/C3-DC
Ci4-DC/C4-DC
C8:1
C8
C5-DC
C6:1-DC/C8:1-OH
C6-DC
C10:3
C10:2
C10:1
C10
C7-DC
C8:1-DC
C10-OH/C8-DC
C12:1
C12
C12-OH/C10-DC
C14:2
C14:1
C14
C14:1-OH/C12:1-DC
C14-OH/C12-DC
C16:2
C16:1
C16
C16:1-OH/C14:1-DC
C16-OH/C14-DC
C18:2
C18:1
C18
C18:2-OH
C18:1-OH/C16:1-DC
C18-OH/C16-DC
C20:4
C20
C20:1-OH/C18:1-DC
C20-OH/C18-DC
C22

Figure 5

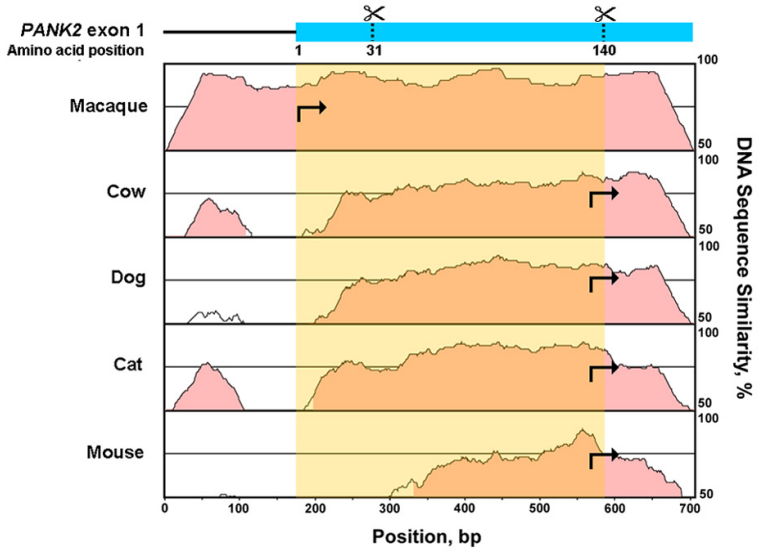

Figure 6

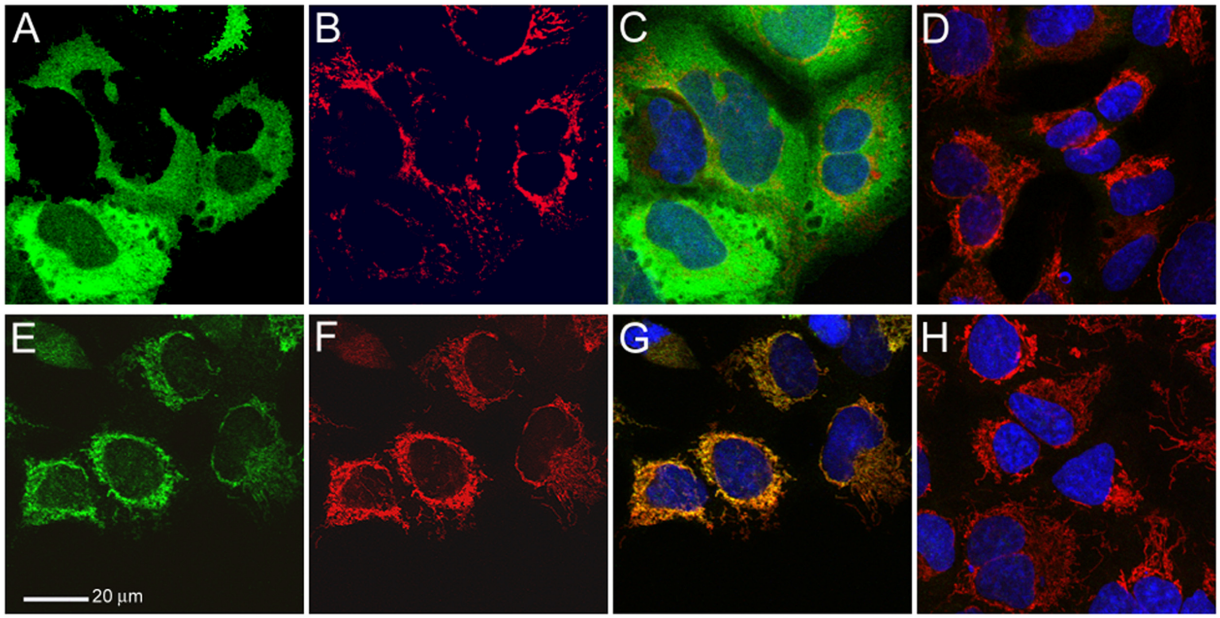

Figure 7

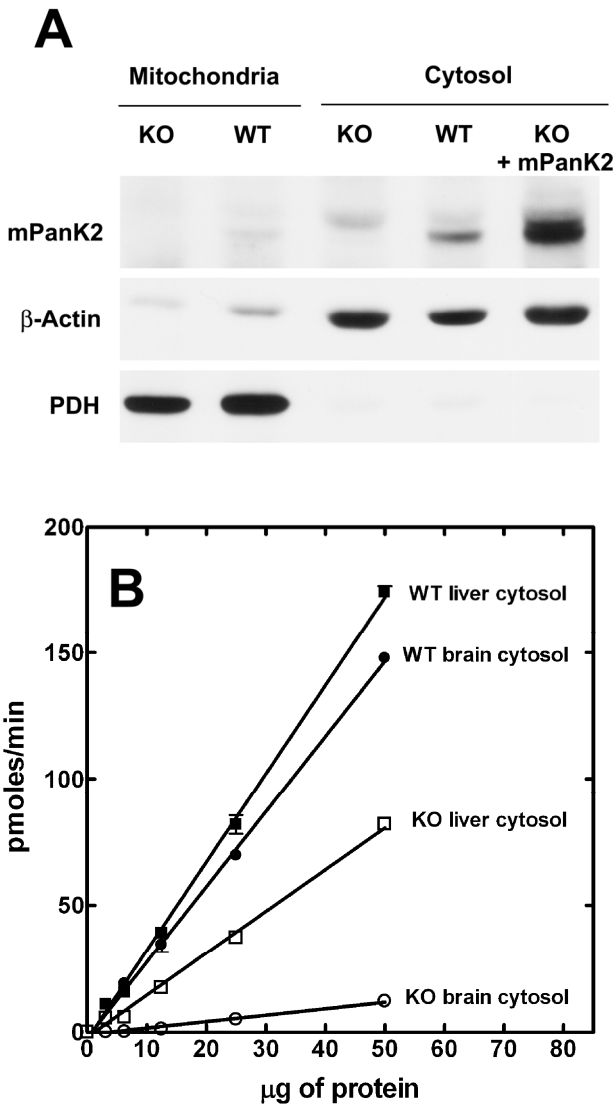
A
Mitochondria
Cytosol
KO
WT
KO
WT
KO
+ mPanK2
mPanK2
β-Actin
PDH
B
WT liver cytosol
WT brain cytosol
KO liver cytosol
KO brain cytosol
pmoles/min
μg of protein
0
50
100
150
200
0
10
20
30
40
50
60
70
80

Figure 8